Effect of Nucleating Agent on the Nonisothermal Crystallization Kinetics of Glass Fiber- and Mineral-Filled Polyamide-6 Composites

Selen Şanlı,[1] Ali Durmus,[2] Nevra Ercan[2]

[1]*EPSAN Plastics, Department of R&D, Ali Osman Sönmez Cad. No:16, Bursa, Turkey*
[2]*Department of Chemical Engineering, Engineering Faculty, Istanbul University, 34320 Avcilar, Istanbul, Turkey*

Received 3 August 2011; accepted 3 October 2011
DOI 10.1002/app.36231
Published online 14 January 2012 in Wiley Online Library (wileyonlinelibrary.com).

ABSTRACT: In this study, nonisothermal crystallization kinetics of glass fiber (GF) and clay-type mineral (MN)-reinforced polyamide-6 (PA6) composites prepared in a twin screw extruder were investigated by differential scanning calorimetry method in the presence and absence of an organic nucleating agent (NA). Kinetic parameters for the nonisothermal melt-crystallization process of samples were determined with several models namely Ozawa, Avrami, Jeziorny, and Liu–Mo. Crystallization rate parameters of the samples and nucleation activity of the fillers and additives were also calculated by the models suggested by Zhang and Dobreva and Gutzow, respectively. Crystallization activation energies of the samples were determined by the Kissinger model. It was found that the MN filler accelerates dramatically the crystallization rate of PA6 even without a NA. Small amount of NA also has a significant acceleration effect on the crystallization rate of PA6 composites. The rate acceleration effect of NA was found to be more pronounced in the composite sample reinforced with GF. Based on the kinetic study using of GF as major filler and small amount of clay-like MN in the PA6 composites could improve the mechanical properties and crystallization rate of injection-molded parts. © 2012 Wiley Periodicals, Inc. J Appl Polym Sci 125: E268–E281, 2012

Key words: polyamides; composites; mineral; crystallization; differential scanning calorimetry

INTRODUCTION

Polyamide-6 (PA6), the most widely used member of aliphatic polyamides in many engineering applications such as automotive parts, electronic equipments, and packaging materials due to its superior physical and mechanical properties shows interesting crystalline features. It exhibits two crystalline structures, namely, α and γ phases.[1] It is known that crystalline structure of PA6 can be influenced by thermal conditions, stress, moisture, and additives.[2,3] Injection-molded parts produced from PA6 compounds which include various types of additives such as impact modifiers, fillers, nucleating agents (NA), etc., are commonly used in automotive plastics. The most widely used commercial fillers in the PA6 compounds are short glass fiber (GF) and minerals (MN) for enhancing of mechanical properties and cost-saving manufacturing of complex parts. Therefore, comprehensive knowledge of the material considering the structure–property relationships is essential for an appropriate and economical design. Many articles have been published about the investigation of mechanical properties of GF-reinforced PA6 composites[4–10] and nanocomposites[11–13] in both computational and experimental point of view.

It is well known that physical properties of a semicrystalline polymer are governed by the supramolecular structure, which in turn is controlled by the crystallization. Crystallization behavior of PA6 compounds and composites not only depends on the structural features of the matrix but also physical properties of the second phase and/or fillers such as surface character, loading amount, geometry, dispersion, etc., and processing conditions. In the last decade, many research efforts have been devoted into studying the effects of various types of nanofillers such as carbon nanotubes,[14–16] graphite[17] and clays/organoclays,[18–20] and nanotubular halloysite[21] on the crystallization behavior of polyamides. On the other hand, crystallization behaviors of polyamide blends have also been studied.[22,23] Wu et al. studied the nonisothermal crystallization kinetics and melting behaviors of PA6 matrix in PA6/PA66 blend, namely, all-PA composites and reported that the nucleation mechanism, crystal growth, and final crystal form of PA6 were changed by the presence of PA66 fibers in the all-PA composites.[24] The use of NA is mostly essential in industrial processing operations to control the structure formation and to shorten the cycle time especially in case of slowly

Correspondence to: A. Durmus (durmus@istanbul.edu.tr).

TABLE I
Some Physical Properties and Chemical Composition of the Mineral Filler

pH	5.5
Loss of ignition (wt %)	8.40
Cation exchange capacity (CEC)	82 meq/100 g
Particle size analysis (μm)	(wt %)
>140	1
140–70	12
70–40	10
<40	77
Chemical composition	
SiO_2	61.16
Al_2O_3	19.44
CaO	0.38
Fe_2O_3	4.60
MgO	2.26
Na_2O	0.22
K_2O	2.05

crystallized polymers such as poly(ethylene terephthalate) and PA6. Effect of NA, generally β-nucleants, on the crystallization behavior polyamide blends were studied in the polypropylene (PP)/polyamide blends for the crystallization of PP phase rather than polyamide.[23,25–29]

To the best of our knowledge, only Göschel et al.[30] investigated the influence of a polymeric nucleating additive on the crystallization of GF-reinforced PA6 composite. They investigated the effects of different amounts (0.1 and 0.2 wt %) of a polymeric nucleating additive based on the short-chain polyamide 2,2 on the crystallization kinetics and morphology of short glass fiber-reinforced PA6 composites by the differential scanning calorimetry (DSC), optical hot-stage microscopy and atomic force microscopy methods. They reported that the polymeric NA had a minor influence on the orientation of GFs but significantly increased the overall crystallization rate of PA6. It was also pointed out that the polymeric NA significantly enhanced the heat deflection temperature of PA6-GF composite possibly due to an improved fiber-to-matrix contact in relation to the spherulite size and distribution.

In this study, nonisothermal crystallization kinetics of GF- and natural clay-reinforced PA6 composites were investigated by DSC method in the presence and absence of an organic NA. Crystallization data were quantified to understand rate acceleration effect of the NA for the crystallization of PA6 composites reinforced with the most widely used commercial fillers, GF, and natural MN. This quantification has provided important knowledge for the injection-molding operations in plastic industry.

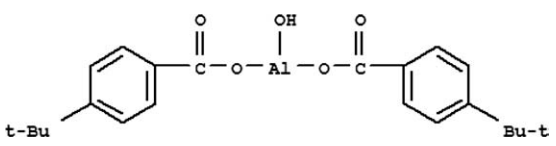

Figure 1 Chemical formula of the nucleating agent.

TABLE II
Sample Compositions

Samples	wt % Polyamide-6 (PA6)	wt % Glass fiber (GF)	wt % Mineral fiber (MN)	phr Nucleating agent (NA)
PA6	100			
PA6-GF	85	15		
PA6-GF-NA	85	15		0.5
PA6-MN	85		15	
PA6-MN-NA	85		15	0.5

EXPERIMENTAL

Materials

In this study, PA6, Akulon® F232 supplied from DSM was used as composite matrix. GF used in the study was a commercial grade chopped strand obtained from Şisecam, TR. It is a surface-treated GF (PA2) with a silane-based coupling agent (0.6 ± 0.15 wt %) and recommended for the polyamide-based composites. The chopped length and filament diameter of PA2 have been declared as 3 mm and 10.5 μm by the producer, respectively. MN filler used in the study was natural clay, denoted by a local supplier. Physical properties of the MN filler were given in Table I. NA used in the study is Sandostab® 4030 supplied from Clariant. It is bis(*p-tert*-butyl benzoate)hydroxyaluminum in white, fine, and free-flowing powder form, having the chemical formula of $C_{22}H_{27}AlO_5$ with the density of 1.14 g cm^{-3}. The chemical structure of Sandostab® 4030 is given in Figure 1.

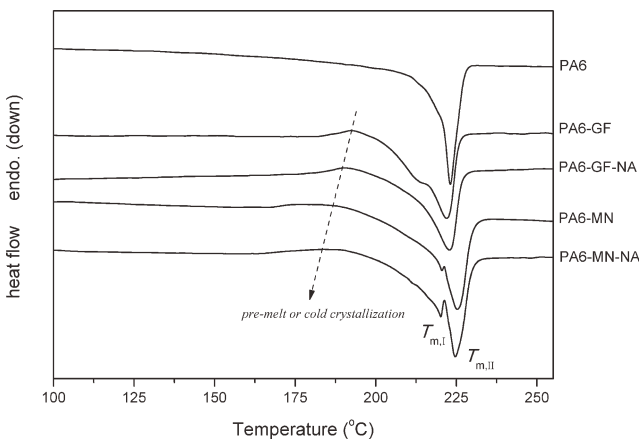

Figure 2 First melting endotherms of the PA6 and composite samples recorded at the heating rate of 10°C min^{-1}.

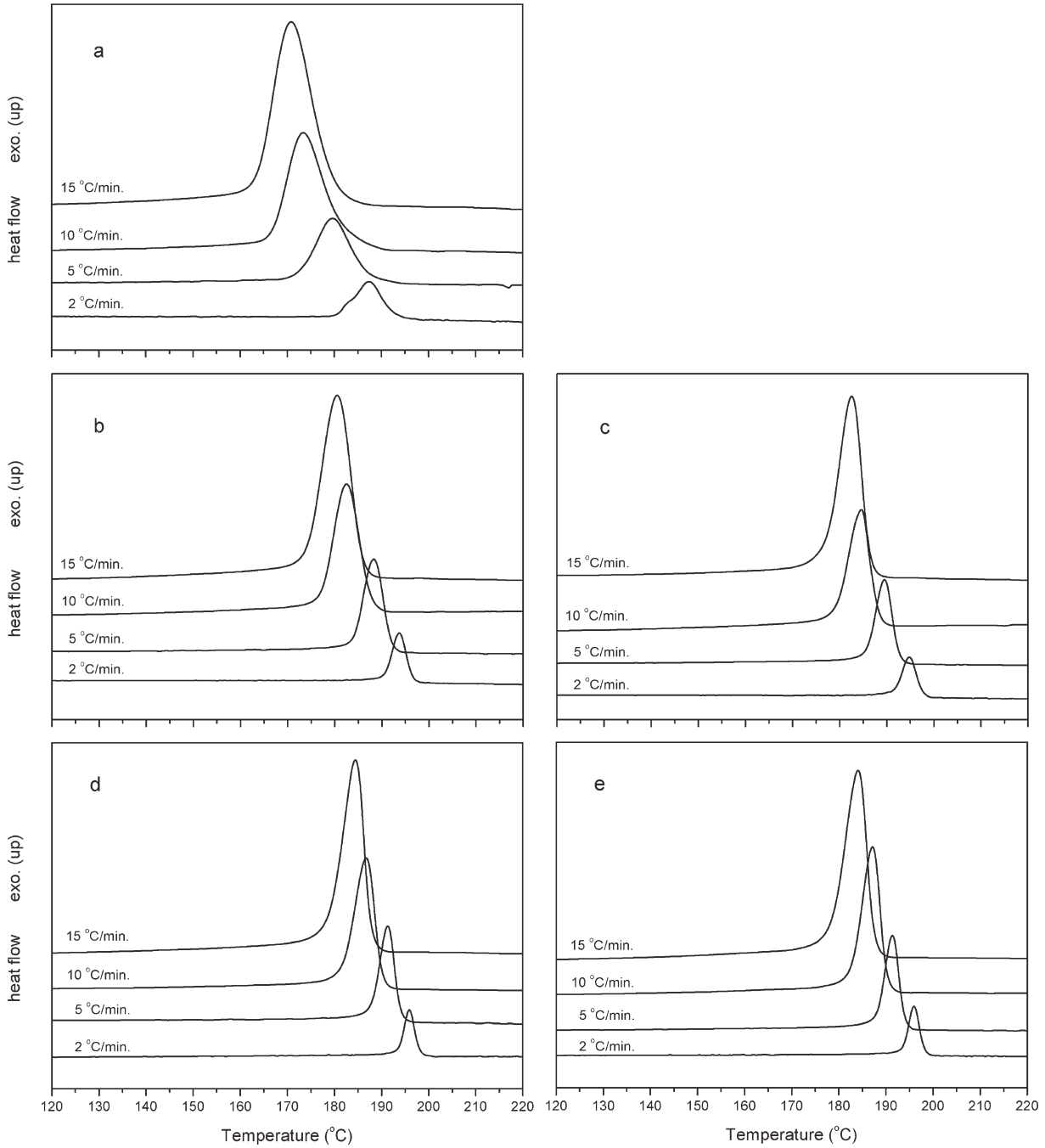

Figure 3 Nonisothermal crystallization exotherms of the samples. (a) PA6, (b) PA6-GF, (c) PA6-GF-NA, (d) PA6-MN and (e) PA6-MN-NA.

Melt processing

Samples were processed in a lab-scale twin screw extruder (Coperion, ZSK 26 MC, *D*: 26 mm, *L*/*D*: 40) with a screw speed of 80 rpm. A temperature profile of 250–280°C was applied throughout the barrel from the feeding zone to die and then the extrudate was granulated. PA6 was also processed at the same conditions. Before the melt processing, PA6 granules and fillers were dried in a vacuum oven overnight at 70°C. Sample compositions are defined in Table II. Extrudated granules were kept in moisture barrier aluminum sachets to prevent possible effects of humidity on the crystallinity of PA6 and composite samples.

Differential scanning calorimetry (DSC) study

Melting and crystallization runs of the samples were carried out in a heat flux-type DSC, SII Nanotechnology ExStar 6200. Temperature and heat flow

calibration of the instrument were achieved with high purity indium (In), tin (Sn), and zinc (Zn) metals.

In nonisothermal crystallization runs, samples weighing about 9–10 mg in an aluminum crucible were heated from 0 to 260°C with the heating rate of 10°C min^{-1} and kept at this temperature for 2 min to remove the thermal history then cooled from 250 to 0°C with the cooling rate of 2, 5, 10, and 15°C min^{-1} by an electrical cooling device, Thermo Scientific EK90C/SII intracooler. After completion of the melt-crystallization process, samples were kept at 0°C for 2 min. Subsequently, nonisothermally crystallized samples at different cooling rates were heated again from 0 to 260°C with the heating rate of 10°C min^{-1}.

Degree of crystallinity (X_c) was determined from the second melting enthalpy values using the following equation:

$$X_c(\%) = \frac{\Delta H_m}{(1-\alpha)\Delta H_m^0} \times 100 \quad (1)$$

where ΔH_m is second melting enthalpy of the samples (J g^{-1}), ΔH_m^o is the enthalpy value of melting of a 100% crystalline form of PA6 (240 J g^{-1}),[31] and α is the total weight fraction of fillers and additives. All runs were carried out under nitrogen (N_2) atmosphere at a flow rate of 50 mL min^{-1} to prevent thermal degradation of the samples.

RESULTS AND DISCUSSION

First melting endotherms of the samples

Figure 2 shows the first melting endotherms of the PA6 and composite samples recorded at the heating rate of 10°C min^{-1}. A clear premelt crystallization exotherm is observed for the composite samples before the melting at the heating rate used. Premelt crystallization behavior can be attributed to formation of smaller crystals within the amorphous region or rearrangement of disordered or uncompleted crystals by the chains which gain mobility at the temperatures before melting. This behavior is more pronounced in the PA6-GF composites. It was found that premelt crystallization peak temperatures of PA6-GF, PA6-GF-NA, PA6-MN, and PA6-MN-NA are 192.4, 190.5, 179.3, and 184.0°C, respectively. As seen, organic NA slightly decreased the premelt crystallization peak temperature in the PA6-GF sample while it increased this temperature in the PA6-MN system. On the other hand, double melting endotherms, which are known as the characteristic behavior of PA6, are seen for the composite samples except the PA6-GF-MN. Double melting behavior will be discussed later regarding the sample composition and nonisothermal crystallization conditions as it mainly depends on the compositional parameters and thermomechanical history of the samples.

TABLE III
Melt Crystallization Onset (T_{co}) and Peak (T_{cp}) Temperatures, Crystallization Rates, and Enthalpy Values of the Samples

Samples	ϕ (°C min^{-1})	T_{co} (°C)	T_{cp} (°C)	$\tau_{0.5}$ (min^{-1})	[a]ΔH_c (J g^{-1})
PA6	2	193.6	187.4	0.17	56.7
	5	187.7	179.6	0.32	63.5
	10	184.2	173.5	0.59	66.5
	15	181.0	170.8	0.91	65.2
PA6-GF	2	196.7	193.7	0.37	49.0
	5	192.5	188.3	0.71	51.6
	10	188.2	182.6	0.93	54.4
	15	186.2	180.7	1.56	52.2
PA6-GF-NA	2	198.1	194.8	0.40	52.5
	5	193.1	189.5	0.76	48.7
	10	188.8	184.6	1.26	46.4
	15	186.6	182.5	1.70	53.9
PA6-MN	2	198.2	195.9	0.45	54.1
	5	194.2	191.3	0.73	57.0
	10	190.3	186.7	1.33	57.2
	15	188.3	184.3	1.80	58.0
PA6-MN-NA	2	198.3	196.0	0.42	55.2
	5	194.3	191.4	0.74	57.3
	10	190.5	187.1	1.32	58.6
	15	187.7	184.2	1.61	62.2

[a] Enthalpy of melt-crystallization.

Kinetics of nonisothermal crystallization

Nonisothermal melt crystallization exotherms of the samples at various cooling rates are given in Figure 3(a–e). The crystallization onset (T_{co}) and peak temperatures (T_{cp}) of the samples at which the crystallization rate is maximum at all cooling rates are listed in Table III. As expected, the T_{cp} values shift to lower temperatures with an increasing cooling rate for all the samples. At a given cooling rate, the T_{cp} values of the samples decreased in the order of PA6-MN-NA ≡ PA6-MN > PA6-GF-NA > PA6-GF > PA6.

The most used kinetic approach for the nonisothermal crystallization process of semicrystalline polymers is the Ozawa model.[32] It is based on the extended form of the Avrami approximation assuming that the nonisothermal crystallization process is composed of small isothermal steps. The Ozawa equation is as follows:

$$X_t = 1 - \exp\left(\frac{-K(T)}{\phi^m}\right) \quad (2)$$

where X_t is the relative crystallinity, $K(T)$ is the crystallization rate function, ϕ is the cooling rate (°C min^{-1}), and m is the Ozawa constant which depends on the dimensions of the crystal growth and the nucleation mechanism.

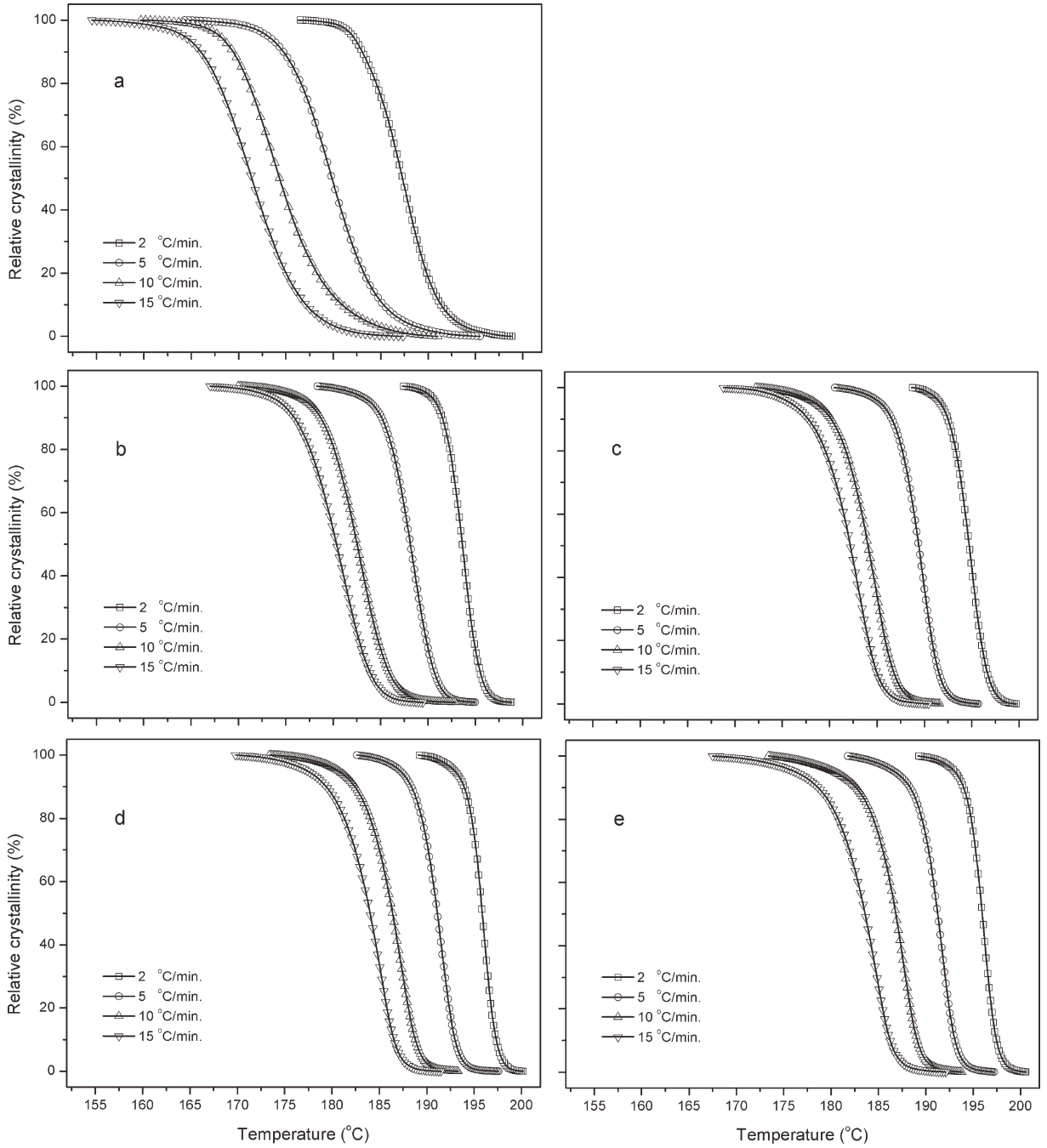

Figure 4 Relative crystallinity (X_t)–temperature curves of the samples. (a) PA6, (b) PA6-GF, (c) PA6-GF-NA, (d) PA6-MN, and (e) PA6-MN-NA.

The relative crystallinity (X_t) as a function of the crystallization temperature or time can be obtained by partial integration of the crystallization exotherms. The relative crystallinity can be defined as a function of the crystallization temperature in the following form:

$$X_t = \frac{\int_{T_o}^{T} \left(\frac{dH_c}{dT}\right) dT}{\int_{T_o}^{T_\infty} \left(\frac{dH_c}{dT}\right) dT} \quad (3)$$

where T_o and T are the onset and end temperatures of the crystallization, respectively. Relative crystallinity (X_t)-temperature (T) curves of the samples are presented in Figure 4(a–e). Figure 5(a–e) shows the X_t-time (t) plots of the samples. All the X_t–t curves at various cooling rates have the same characteristic sigmoid shape. The first nonlinear part of the S-shaped curves is generally considered as the nucleation step of the crystallization process. Each curve showed a linear part considered as primary crystallization; subsequently a second nonlinear part

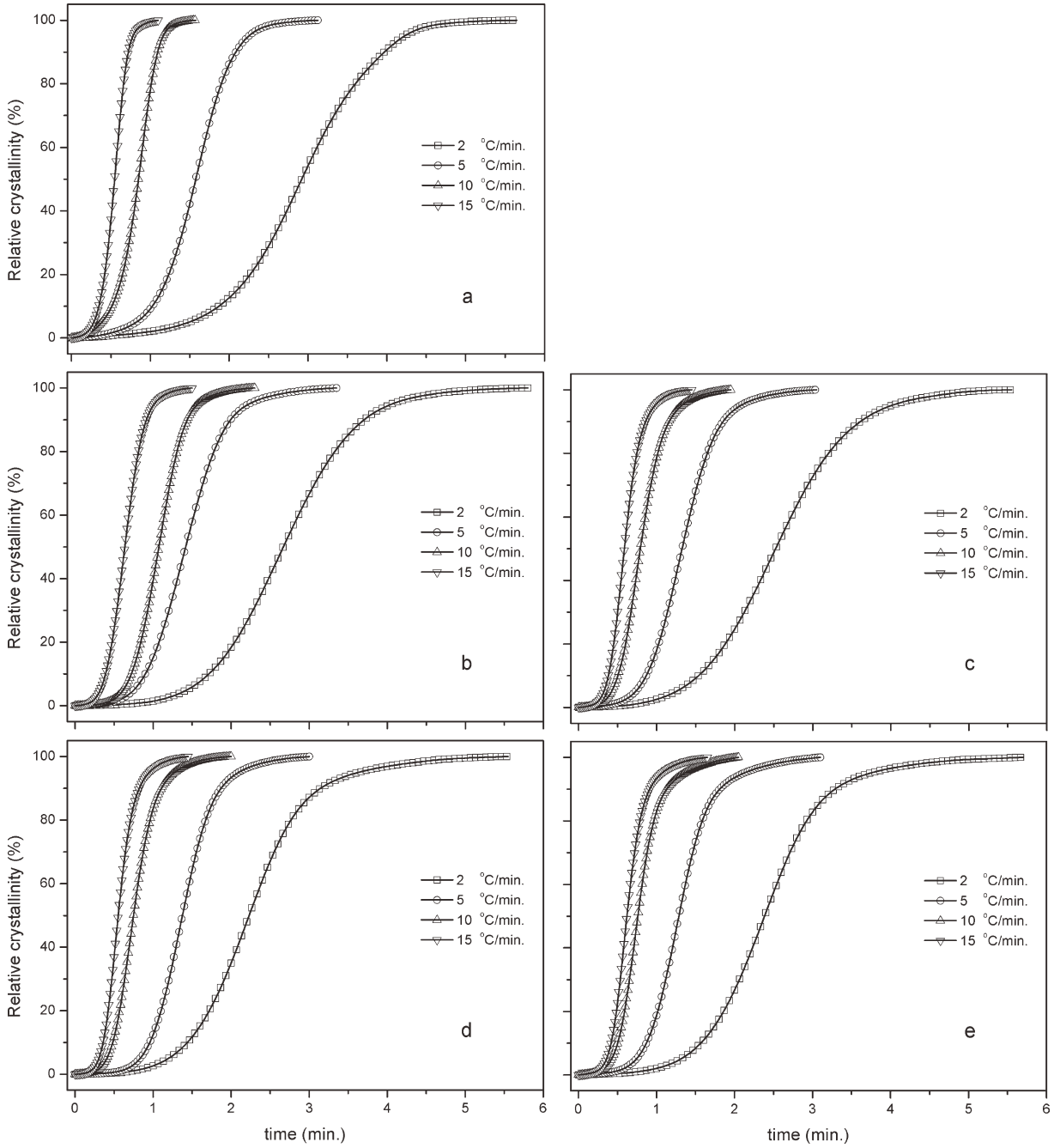

Figure 5 Relative crystallinity (X_t)–time curves of the samples. (a) PA6, (b) PA6-GF, (c) PA6-GF-NA, (d) PA6-MN, and (e) PA6-MN-NA.

deviated off slightly and is considered secondary crystallization, which was caused by the spherulite impingement in the late stage of the crystal growth. For the relative crystallinity versus time (t) curves, a higher cooling rate led to a shorter time to complete the crystallization.

If the double logarithmic form of the eq. (2) is taken, a linear relationship can be obtained as follows:

$$\ln[-\ln(1 - X_t)] = \ln K(T) - m\ln\varphi \quad (4)$$

Plotting ln [–ln (1–X_t)] against lnϕ at a given temperature should yield a straight line. The slope of the line is the Ozawa constant, m, and the intercept is $K(T)$. Ozawa plots of the PA6 are given in Figure 6(a). The Ozawa model successfully fitted the nonisothermal crystallization behavior of the PA6 at various crystallization temperatures. Figure 6(b) shows the Ozawa plots of nucleated and non-nucleated composite samples at 186°C. It is clearly seen that Ozawa model cannot fit the nucleated and non-nucleated MN filled composites. Similarly, it has

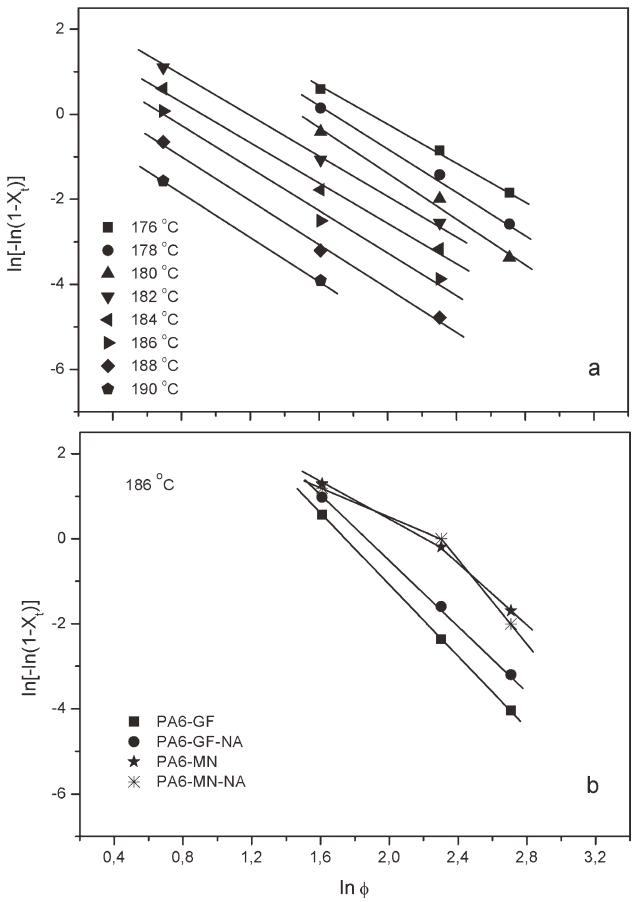

Figure 6 Ozawa plots of the samples. (a) PA6 and (b) Composite samples at 186°C.

been reported that the Ozawa equation could not be used for modeling of the nonisothermal crystallization kinetics of some polymer/clay nanocomposite systems.[33–35] The Ozawa kinetic parameters for the crystallization process of the PA6 and composite samples including GF are listed in Table IV. The m values of the PA6 varied between 2.20 and 2.65 which suggest the homogeneous nucleation and growth mechanism of the combination of two dimension (2D) and three dimension (3D). On the other hand, m was found to be 4.20 and 3.79 for the PA6-GF and PA6-GF-NA, respectively, which refer these samples were heterogeneously nucleated and growth in 3D. The $K(T)$ values of the PA6 decreases with the increasing of temperature as expected. However, it is seen that the $K(T)$ values of the nucleated and non-nucleated composites reinforced with the GF are dramatically higher than that of PA6 at 186°C. This result demonstrates the rate acceleration effect of GF and NA used in the study on the crystallization of PA6.

An alternative approach, the Avrami model,[36–38] was used in this study to compare crystallization rates of the samples. The Avrami equation is as below:

$$X_t = 1 - \exp(-Z_t t^n) \tag{5}$$

where n is the Avrami constant which depends on the crystal growth mechanism and Z_t is the rate constant involving both nucleation and growth rate parameters. The Avrami model is generally used to analyze the isothermal crystallization kinetics of a polymer taking into account the developing relative crystallinity with time. Therefore, it should be noted that in nonisothermal crystallization, the Avrami kinetic parameters do not have the same physical meanings as in the isothermal crystallization since the temperature changes steadily in the nonisothermal processes. Both nucleation and crystal growth processes are temperature dependent in the nonisothermal crystallization. However, the Avrami model can provide useful insights into the kinetics of nonisothermal crystallization processes. Taking double logarithmic form of the eq. (5):

$$\ln[-\ln(1 - X_t)] = \ln Z_t + n \ln t \tag{6}$$

and plotting ln[–ln(1–X_t)] versus ln$t$ for each cooling rate, straight line should be obtained to determine kinetic constants. Avrami plots generally fit the experimental data linearly at low degree of crystallinity and deviate from the linear regression at higher crystallization ratio as possible; it does not account the secondary crystallization. In nonisothermal crystallization, the temperature change at a given cooling rate affects the rate of both nucleation and spherulite growth which are temperature-dependent parameters. Considering the temperature-dependent character of the nonisothermal crystallization process, the rate parameter, Z_t, was modified by Jeziorny.[39]

$$\ln Z_c = \frac{\ln Z_t}{\phi} \tag{7}$$

Avrami plots of the samples are illustrated in Figure 7 and the kinetic constants obtained by the Jeziorny modification are listed in Table V. As shown in Figure 7, the Avrami model was able to fit the

TABLE IV
Ozawa Kinetic Parameters of the Samples

Samples	Temperature (°C)	m	$K(T)$ [(°C min^{-1})^m]	r^2
PA6	176	2.20	64.37	0.996
	178	2.46	63.06	0.992
	180	2.65	50.36	0.975
	182	2.28	14.26	0.998
	184	2.36	8.77	0.990
	186	2.47	5.45	0.982
	188	2.58	2.98	0.994
	190	2.56	1.22	1.000
PA6-GF	186	4.20	1506	0.999
PA6-GF-NA	186	3.79	1207	0.999

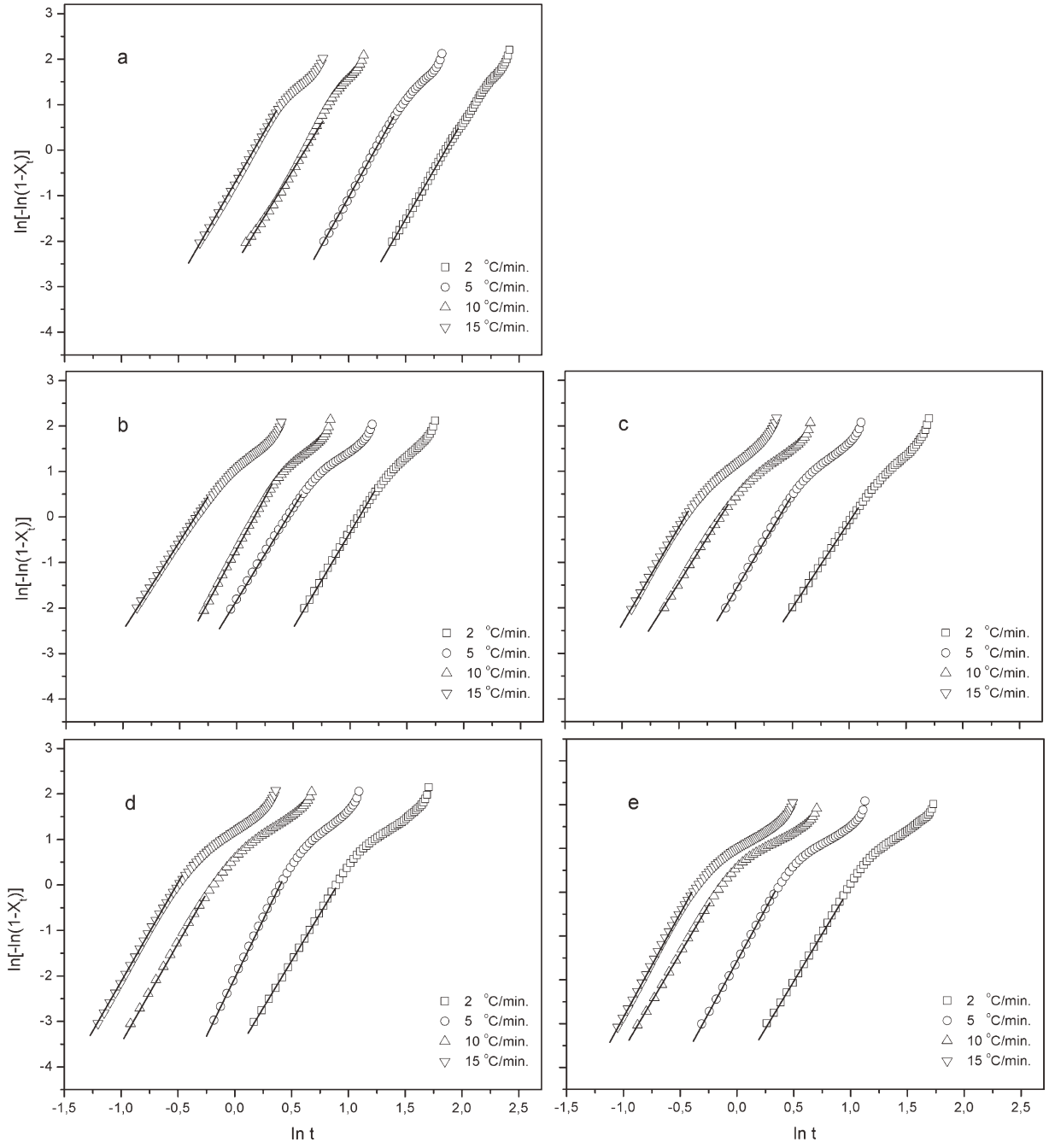

Figure 7 Avrami plots of the samples. (a) PA6, (b) PA6-GF, (c) PA6-GF-NA, (d) PA6-MN, and (e) PA6-MN-NA.

primary crystallization stage of the samples and it deviated from linearity due to the secondary crystallization for all cooling rates. Changes in Avrami constants (n) with cooling rate imply that crystallization of the samples occurred in various growth forms. It was found that n values varied depending on the cooling rate and type of filler. Consequently, it is difficult to infer the nucleation mechanism and crystal growth analysis based on the Avrami constants of the samples. On the other hand, the rate parameters (Z_c) of the samples increase with the increasing of cooling rate for all samples. At a given cooling rate, especially relatively high cooling rates (e.g., 10 and 15°C min^{-1}) which can provide inferential knowledge for the real solidification conditions in the plastic processing operations, Z_c values of the samples decreased in the order of PA6-MN>PA6-MN-NA>PA6-GF-NA>PA6-GF>PA6. This relationship denotes that the clay-like MN can act a very efficient filler to increase the crystallization rate of PA6.

Another method, developed by Liu and Mo,[40] was also used to describe the nonisothermal melt-crystallization process. Liu et al. offered a new method

TABLE V
Avrami–Jeziorny Kinetic Parameters

Samples	ϕ (°C min^{-1})	n	Z_c (min^{-1})	r^2
PA6	2	4.13	0.021	0.998
	5	4.69	0.316	0.997
	10	4.67	0.753	0.998
	15	4.36	0.951	0.998
PA6-GF	2	4.32	0.101	0.999
	5	4.07	0.699	0.997
	10	3.88	0.944	0.999
	15	3.66	1.087	0.998
PA6-GF-NA	2	3.81	0.142	0.998
	5	4.00	0.741	0.996
	10	4.06	1.058	0.997
	15	4.35	1.141	0.998
PA6-MN	2	4.02	0.157	0.998
	5	5.30	0.668	0.998
	10	4.36	1.099	0.999
	15	4.32	1.157	0.997
PA6-MN-NA	2	4.22	0.127	0.999
	5	4.72	0.730	0.998
	10	4.41	1.085	0.998
	15	4.90	1.145	0.999

combining the Avrami and Ozawa equations at a given value of X_t as follows:

$$\ln K(T) - m \ln \phi = \ln Z_t + n \ln t \quad (8)$$

$$\ln \phi = \ln F(T) - a \ln t \quad (9)$$

where the parameter $F(T)=[K(T)/Z_t]^{1/m}$ refers to the cooling rate, and a is the ratio of the Avrami constant n, to the Ozawa constant m. According to the Liu–Mo model, plotting lnϕ versus ln$t$, series of straight lines are obtained at a given value of relative crystallinity. The kinetic parameters, $F(T)$ and a, could be determined by intercept and slope of these lines, respectively. At a certain value of X_t, a higher value of $F(T)$ means that a high cooling rate is needed to reach this X_t in a unit time which also indicates the difficulty in crystallization process. The Liu–Mo plots of the samples are shown in Figure 8(a–e). The Liu–Mo model was applied to the samples at the relative crystallinity values of 20, 40, 60, and 80% and successfully fit the crystallization kinetics of the PA6 and composite samples. Table VI summarizes the values of Liu–Mo parameters for the samples. Values of a increased slightly with the increasing of X_t for all the samples. In Table VI, it is also seen that the $F(T)$ values increase with the developing of X_t. From the Liu–Mo modeling of the samples, the $F(T)$ values of PA6 were found to be the highest at a given relative crystallinity value. This indicates the difficulty for nonisothermal crystallization of PA4 compared to composite samples. At a particular X_t, $F(T)$ values of the samples decreased in the order of PA6>PA6-GF>PA6-GF-NA≡PA6-MN-NA>PA6-MN. This result also implies the efficiency of MN filler to easify and promote the nonisothermal crystallization of PA6.

Another simple and quantitative approach for comparing the effects of fillers and/or additives on the nonisothermal crystallization rate of the samples is to calculate the crystallization rate parameter (CRP) which can be determined from the slope of a linear line drawn through a plot of the reciprocal crystallization half-time ($\tau_{0.5}=1/t_{0.5}$) versus the cooling rate (ϕ).[41,42] Crystallization half-time ($t_{0.5}$) which is defined as the time taken the relative crystallinity of the sample reaches the value of 50% can be directly obtained from the relative crystallinity–time curves. Figure 9 shows the plots of $\tau_{0.5}$ versus ϕ for the samples. The values of CRP are listed in Table VI. The CRP values of the samples increased in the order of PA6<PA6-GF<PA6-GF-NA≡PA6-MN-NA<PA6-MN which refers that the MN filler is the most effective material to enhance the crystallization rate of PA6 even in the absence of NA. The composites that include GF and MN yielded the same CRP values in the presence of NA into the composition. These results are convenient with the kinetic findings mentioned above.

Nucleation activity of fillers and Sandostab® 4030

Dobreva and Gutzow[43,44] suggested a simple method to calculate the nucleation activity of foreign substrates, additives, etc., in a polymer melt. This method has also been used for silica nanoparticle-filled PEN,[45] surface modified talc-PP composites,[46] and PP/SiO_2 nanocomposites.[47] Nucleation activity (φ) can be defined as a factor by which the work of 3D nucleation decreases with the addition of a foreign substrate. If the foreign substrate is extremely active for nucleation, value of φ approaches 0, while it is about 1 for inert particles. Mathematically, the nucleation activity is the ratio of B parameters in heterogeneous and homogenous medium:

$$\varphi = \frac{B^*}{B} \quad (10)$$

B parameter is defined as,

$$B = \frac{\omega \sigma^3 V_m^2}{3 n k_B T_m^0 \Delta S_m^2} \quad (11)$$

where ω is a geometric factor, σ is a specific energy, V_m is the molar volume of the crystallizing substance, n is the Avrami exponent, ΔS_m is the melting entropy, and ΔT_m^0 the equilibrium melting temperature.

However, B parameter could be determined experimentally by using the simple definitions of nonisothermal crystallization. For homogenous nucleation, B parameter can be calculated from the following equation:

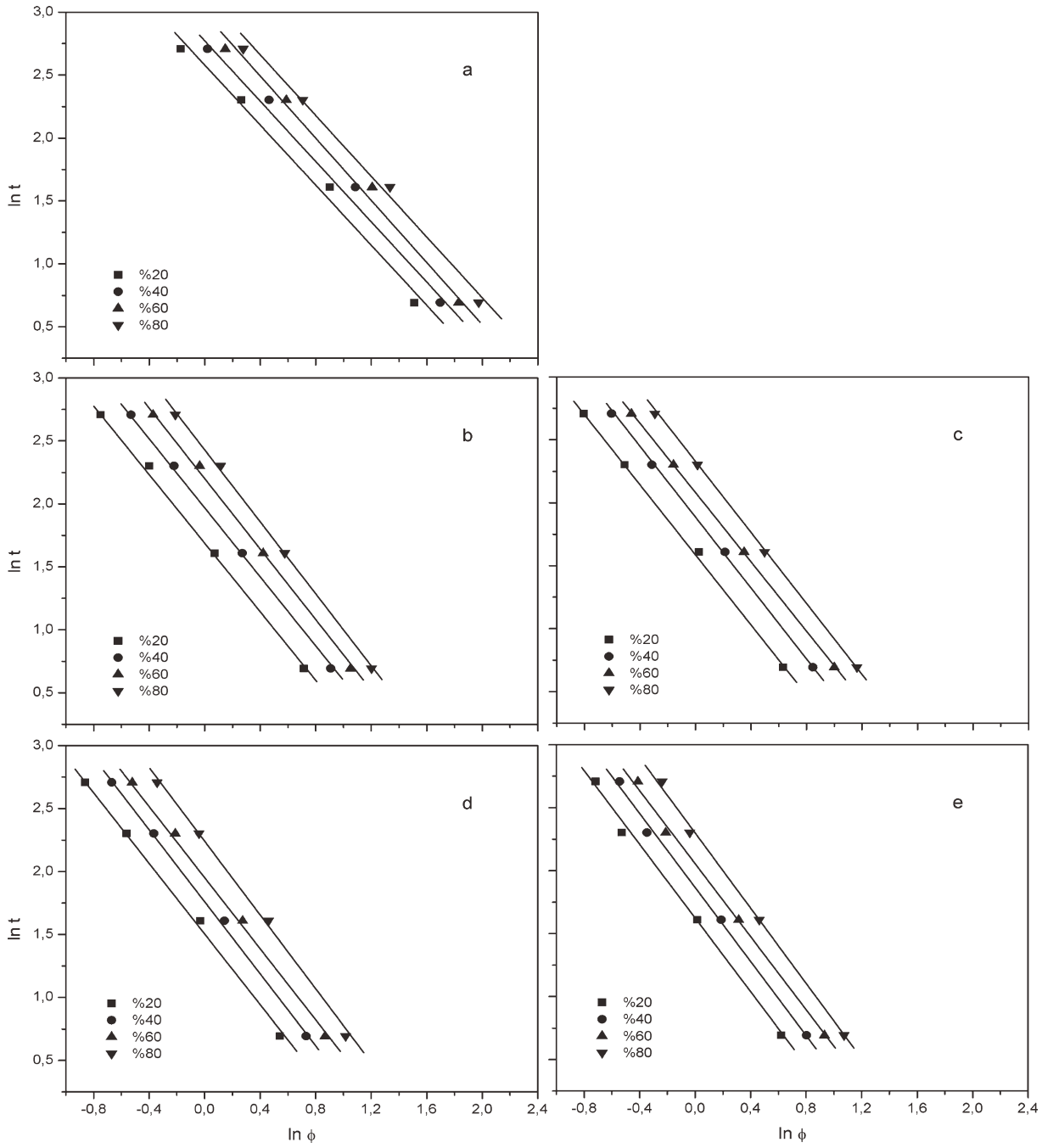

Figure 8 Liu-Mo plots of the samples. (a) PA6, (b) PA6-GF, (c) PA6-GF-NA, (d) PA6-MN, and (e) PA6-MN-NA.

$$\ln \phi = C - \frac{B}{\Delta T_c^2} \tag{12}$$

where ϕ is the cooling rate, C is a constant and ΔT_c is the supercooling ($T_m - T_c$). For heterogeneous nucleation, eq. (12) becomes:

$$\ln \phi = C - \frac{B^*}{\Delta T_c^2} \tag{13}$$

B and/or B^* can be obtained by plotting lnϕ versus the $1/\Delta T_c^2$. These plots of the samples are given in Figure 10. The φ values of the samples are listed in Table VI. As seen, nucleated and non-nucleated MN filled composites exhibit lower φ values than the GF-reinforced counterparts. This can be attributed to the fact that the clay-like MN is more efficient filler than the GF for the nucleation, itself. Furthermore, it could be concluded that the organic NA, Sandostab® 4030, cannot yield an additional decrease in φ for the MN-filled system while it acts an effective nucleants in the composite reinforced with the GF. This could be explained by the fact that the Sandostab® 4030 is mainly located onto the surfaces of clay

TABLE VI
Liu-Mo Kinetic Parameters, Crystallization Rate Parameters (CRP), Nucleation Activity, and Crystallization Activation Energy Values of the Samples

Samples	X_c (%)	a	F (T)	CRP	φ	ΔE_A (kJ mol^{-1})
PA6	20	1.19	13.1	0.057	–	−210.9
	40	1.20	16.6			
	60	1.20	19.2			
	80	1.19	22.2			
PA6-GF	20	1.37	5.4	0.086	0.661	−270.7
	40	1.40	7.2			
	60	1.41	8.9			
	80	1.42	11.2			
PA6-GF-NA	20	1.37	4.9	0.099	0.616	−292.4
	40	1.38	6.5			
	60	1.38	8.0			
	80	1.39	10.0			
PA6-MN	20	1.43	4.5	0.106	0.575	−313.4
	40	1.44	5.9			
	60	1.45	7.2			
	80	1.48	9.3			
PA6-MN-NA	20	1.46	5.0	0.098	0.571	−312.1
	40	1.46	6.5			
	60	1.47	7.8			
	80	1.50	10.0			

layers/particles thereof the filler-polymer interface. A big organic molecule onto filler surface can deteriorate the nucleation and crystallization behavior of the polymer however it can increase the interfacial interactions. We previously reported that natural clay, montmorillonite, exhibited lower φ value than the organically modified counterpart and unmodified clays were more effective than the modified ones to increase the crystallization rate of the system.[48]

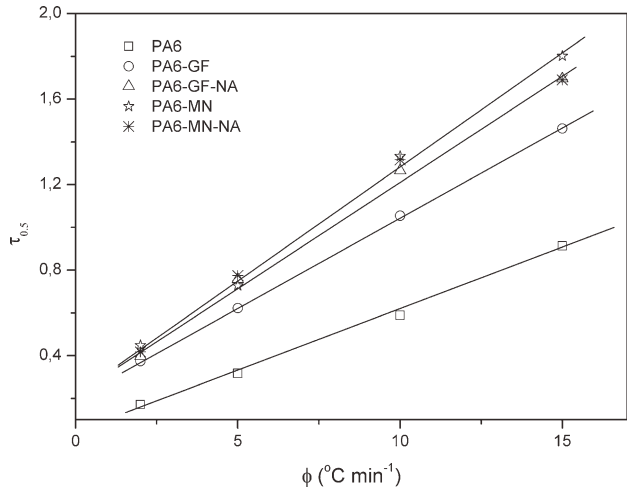

Figure 9 Plots of $\tau_{0.5}$ against the cooling rate, ϕ, for determination of the crystallization rate parameters of samples.

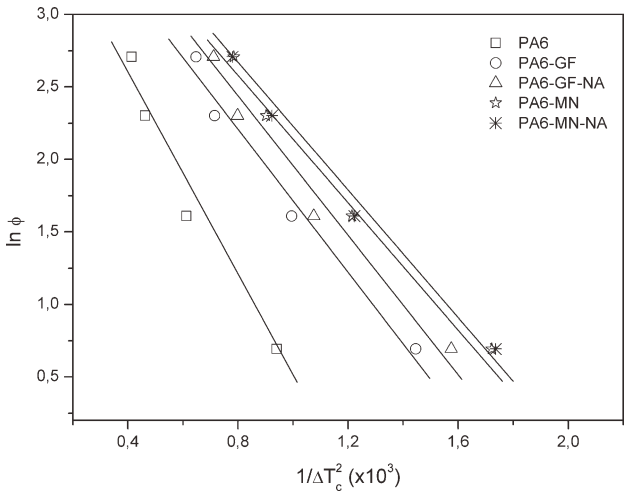

Figure 10 Plots of lnϕ against $1/\delta T_c^2$ for determination of the nucleation activity of fillers.

Crystallization activation energy

Crystallization activation energies of the samples were determined by the Kissinger approach.[49] The Kissinger model, based on the finite relationship between the peak temperatures, T_{cp}, obtained from the nonisothermal crystallization exotherms and the heating/cooling rates used, can be described as follows;

$$\frac{d\left[\ln\left(\frac{\varphi}{T_{cp}^2}\right)\right]}{d\left[\frac{1}{T_{cp}}\right]} = -\frac{\Delta E_A}{R} \tag{14}$$

where ϕ is the cooling rate (°C min^{-1}), T_{cp} is the crystallization peak temperature (K), ΔE_A is the activation energy of the crystallization process (kJ mol^{-1}), and R is the universal gas constant (8.314 kJ mol^{-1}K^{-1}). Kissinger plots of the samples are given in Figure 11, and the ΔE_A values are listed in Table

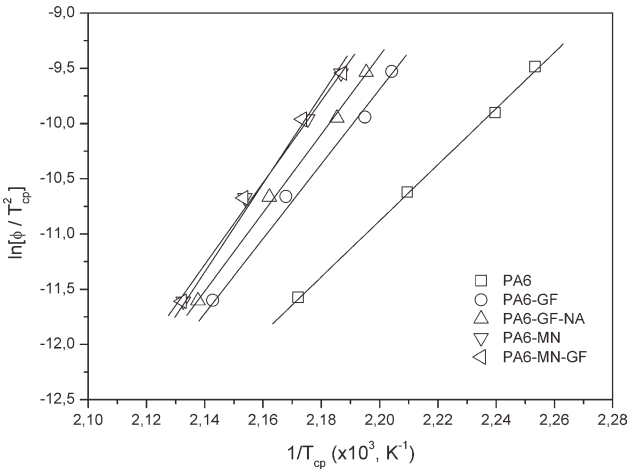

Figure 11 Kissinger plots of the samples.

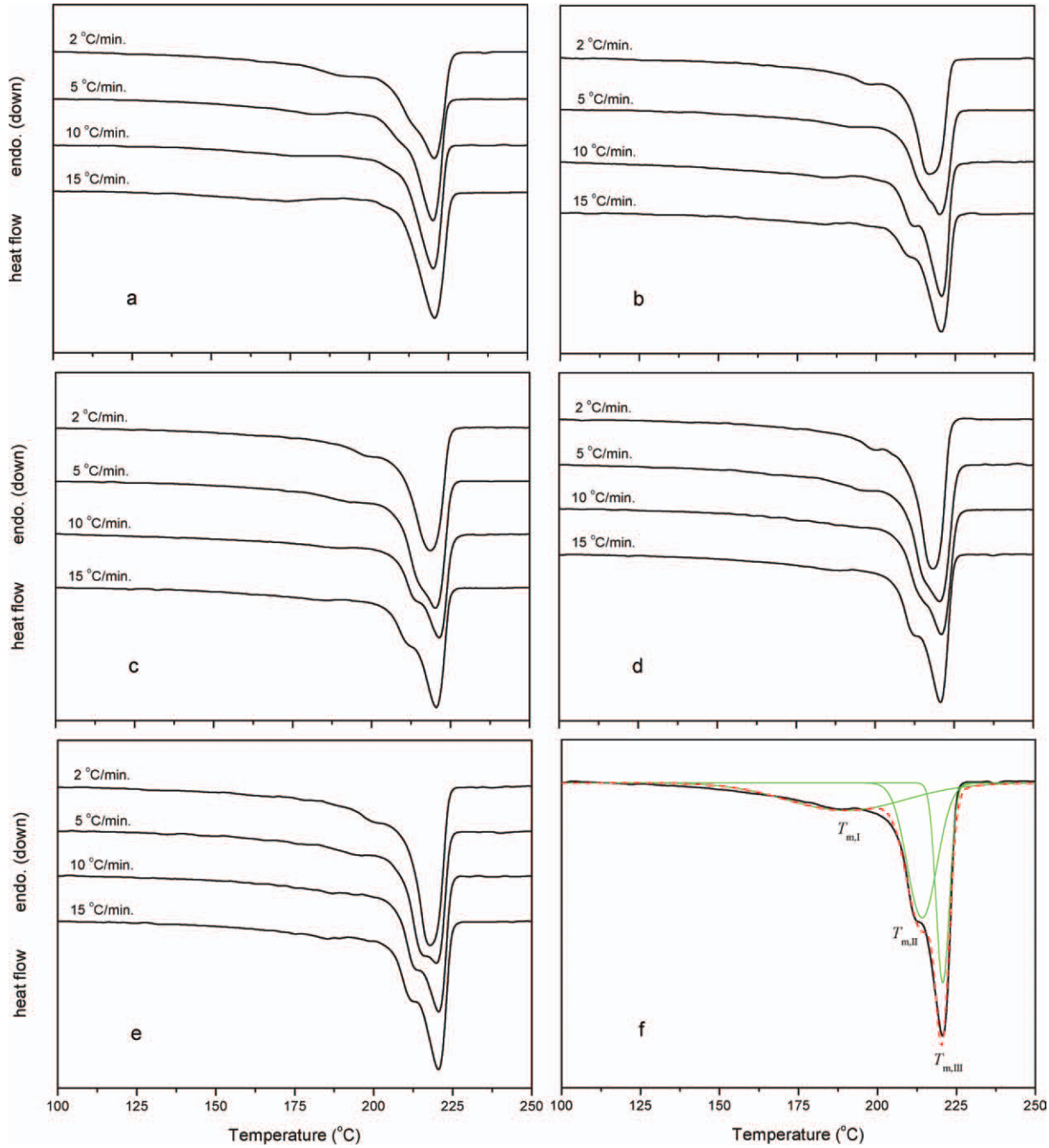

Figure 12 Second melting endotherms of the samples. (a) PA6, (b) PA6-GF, (c) PA6-GF-NA, (d) PA6-MN and (e) PA6-MN-NA. (f) Peak deconvolution of a sample. The solid lines represent the experimental (black) and deconvoluted (green) curves, respectively. The dashed (red) line represents the fitted melting endotherm or sum of the deconvoluted peaks. [Color figure can be viewed in the online issue, which is available at wileyonlinelibrary.com.]

VI. ΔE_A is negative due to the exothermic nature of the transition from melt to crystalline state and the negative activation energy values also imply that the crystallization mechanisms are accelerated by decreasing the temperatures. The ΔE_A values of all the composite samples were significantly lower than PA6. The ΔE_A values of the samples decreased in the order of PA6>PA6-GF>PA6-GF-NA>PA6-MN≡PA6-MN-NA which refers the reducing of energy barrier for crystallization depending on the sample composition.

Second melting behaviors of the samples

In some cases, semicrystalline polymers can exhibit multiple melting endotherms which are generally attributed to the melting of imperfect crystals formed during the crystallization or formation of

TABLE VII
Melting Temperatures, Enthalpy of Fusion, and Degree of Crystallinity Values of the Samples

Samples	ϕ (°C min^{-1})	$T_{m,I}$ (°C)	$T_{m,II}$ (°C)	$T_{m,III}$ (°C)	[a]ΔH_m (J g^{-1})	[b]X_c (%)
PA6	2	194.3	214.8	220.7	65.7	32.2
	5	186.3	213.3	220.0	61.8	30.3
	10	183.7	–	220.2	58.5	28.7
	15	174.0	–	220.6	54.6	26.8
PA6-GF	2	198.3	216.7	–	57.2	28.0
	5	194.2	215.5	221.0	53.2	26.1
	10	185.1	212.0	220.8	49.5	24.3
	15	184.0	210.7	220.5	46.2	22.6
PA6-GF-NA	2	199.7	–	218.6	57.9	28.4
	5	194.0	215.0	220.2	51.8	25.4
	10	190.5	214.2	221.4	49.6	24.3
	15	186.0	212.0	220.5	45.9	22.5
PA6-MN	2	200.2	–	218.3	61.2	30.0
	5	198.2	215.6	220.4	56.6	27.7
	10	194.6	214.5	221.0	55.1	27.0
	15	188.5	212.7	220.7	54.8	26.9
PA6-MN-NA	2	200.4	217.8	–	69.3	34.0
	5	196.7	215.8	219.7	67.9	33.3
	10	194.6	213.4	220.5	64.9	31.8
	15	188.8	212.6	220.5	62.1	30.4

[a] Enthalpy of second melting endotherm recorded at the heating rate of 10°C min^{-1}.
[b] Degree of crystallinity calculated from the enthalpy of second melting.

different crystal types depending on the presence of specific NA and/or thermomechanical history. Multiple melting endotherms have been reported for PA6, PA6 composites and blends, so far.[50,51,15,24]

Second melting endotherms of the PA6 and composite samples crystallized at various cooling rates are given in Figure 12(a–e). The melting peak temperatures, enthalpy of fusion and degree of crystallinity values of the samples are listed in Table VII. As seen in Figure 12, it is apparent that the DSC endotherms of the composite samples which were especially crystallized at higher cooling rates (10 and 15°C min^{-1}), exhibit triple melting peaks. At low cooling rates (2 and 5°C min^{-1}), the low-temperature melting peak are not obvious. Thus, each second melting endotherm was simple deconvoluted into three peaks by a Lorentzian function after performing a linear baseline correction. An illustrative peak deconvolution of a sample is given in Figure 12(f). The smaller peaks shown at low and medium temperatures and the main peak shown at high temperature are referred as the $T_{m,I}$, $T_{m,II}$, and $T_{m,III}$, respectively. In the composite samples, the peak positions of $T_{m,I}$ and $T_{m,II}$ shifted to lower temperatures, while the position of main peak, $T_{m,III}$, did not change with the increasing of cooling rate.

Multiple melting peaks of PA6 have been concluded in different manners, depending on the crystallization conditions. For example, Li et al.[15] studied on the isothermal crystallization kinetics of PA6/carbon nanotube (CNT) nanocomposites and reported triple melting endotherms for the isothermally crystallized samples at the temperature range of 188–200°C. They referred the first, second, and third peaks appeared around 193–206, 212–218, and 220°C, respectively, as the melting endotherms of α-spherulites with different size and level of perfection during the crystallization. On the other hand, Wu et al.[24] reported double melting endotherms for the nonisothermally crystallized PA6 at the cooling rate between 1 and 50°C min^{-1}. They observed a low-temperature peak about 215°C referred as the γ-form and a high-temperature peak about 220 referred as the α-form crystals.

In this study, we do not speculate the double melting peaks in related with the different crystal forms of PA6 as the DSC results should be confirmed with X-Ray diffraction (XRD) study to understand formation and transformation of crystal forms of PA6 depending on the fillers and crystallization conditions. However, it can be noticed that the $T_{m,I}$ values of the samples are just 3–5°C higher than the crystallization peak temperatures at a given cooling rates. Therefore, the $T_{m,I}$ could be attributed to the melting of imperfect and smaller crystals which were possibly formed during the secondary crystallization. It was found that degree of crystallinity, X_c (%) values of the all samples decreased with the increasing of cooling rate. PA6 yielded higher X_c values than the composites except the PA6-MN-NA. This could be attributed to formation of smaller crystals in the composite samples due to heterogeneous

nucleation in the first step of crystallization and less imperfection during the crystal growth. The PA6-MN-NA sample shows a slightly higher X_c values than the both PA6 and other composites at a given cooling rate.

CONCLUSIONS

In this study, nonisothermal crystallization kinetics of PA6 composites reinforced with the same amount (15 wt %) of GF and MN fillers were investigated in detail in the presence and absence of an organic NA, Sandostab® 4030. It was found that both fillers already acted a NA for the crystallization of PA6, but the MN filler more effectively increased the crystallization rate of PA6 than the GF independently on the presence of NA. All the kinetic data determined by several mathematical approaches showed that introducing a small amount of Sandostab® 4030 (0.5 wt %) into the composition easified the crystallization and promoted the crystallization rate of GF reinforced composite significantly, whereas it exhibited no additional effect for accelerating the crystallization rate of MN-filled counterpart.

Based on the results of the study, it has been highlighted that PA6 composites reinforced with the surface-treated GFs and including a small amount of clay-like MN as a cheap and easy-accessible minor filler could yielded the best performance for the injection-molded PA6 parts in engineering applications of PA6 composites because the GF enhances the mechanical properties and the clay-like MN accelerate the crystallization rate dramatically.

References

1. Miyasaka, K.; Ishikawa, K. J Polym Sci Part A-2: Polym Phys 1968, 6, 1317.
2. Matyi, R. J.; Cryst, B.,Jr. J Polym Sci Polym Phys Ed 1978, 16, 1329.
3. Ellis, T. S. Polymer 2003, 44, 6443.
4. Nase, M.; Langer, B.; Schumacher, S.; Grellmann, W. J Appl Polym Sci 2009, 111, 2245.
5. Shojaei, A.; Fereydoon, M. Mater Sci Eng A 2009, 506, 45.
6. Chevali, V. S.; Janowski, G. M. Compos Part A: Appl Sci Manufact 2010, 41, 1253.
7. Bernasconi, A.; Cosmi, F.; Zappa, E. Strain 2010, 46, 435.
8. Cosmi, F. Strain 2011, 47, 215.
9. Ferreno, D.; Carrascal, I.; Ruiz, E.; Casado, J. A. Polym Test 2011, 30, 420.
10. Launay, A.; Maitournam, M. H.; Marco, Y.; Raoult, I.; Szmytka, F. Int J Plast 2011, 27, 1267.
11. Shen, S. Z.; Bateman, S.; McMahon, P.; Dell'Olio, M.; Gotama, J.; Nguyen, T.; Yuan, Q. A. Comp Sci Technol 2010, 70, 2063.
12. Zhang, L.; Yang, J. M.; Feng, C. W.; Li, C. Z. Acta Polym Sinica 2010, 11, 1333.
13. Yoo, Y.,Spencer, M. W.; Paul, D. R. Polymer 2011, 52, 180.
14. Wang, B.; Sun, G.; Liu, J.; He, X.; Li, J. Appl Polym Sci 2006, 100, 3794.
15. Li, J.; Fang, Z.; Zhu, Y; Tong, L.; Gu, A.; Liu, F. J Appl Polym Sci 2007, 105, 3531.
16. Yang, Z.; Huang, S.; Liu, T. J Appl Polym Sci 2011, 122, 551.
17. Liu, Y.; Yang, G. Thermochim Acta 2010, 500, 13.
18. Kang, X.; Suqin He, S.; Chengshen Zhu, C.; Wang, L.; Lü, L.; Guo, J. J Appl Polym Sci 2005, 95, 756.
19. Li, Y.; Shimizu, H. J Polym Sci B Polym Phys 2006, 44, 284.
20. Hedicke, K.; Wittich, H.; Mehler, C.; Gruber, F.; Altstädt, V. Compos Sci Technol 2006, 66, 571.
21. Guo, B. C.; Zou, Q. L.; Lei, Y. D.; Du, M. L.; Liu, M. X.; Jia, D. M. Thermochim Acta 2009, 484, 48.
22. Cui, L.; Yeh, J. T.; Wang, K.; Fu, Q. J Polym Sci Part B Polym Phys 2008, 46, 1360.
23. Li, J.; Wang, S. W.; Yang, W.; Xie, B. H.; Yang, M. B. J Appl Polym Sci 2011, 121, 554.
24. Wu, B.; Gong, Y.; Yang, G. J Mater Sci 2011, 46, 5184.
25. Zhang, R. H.; Shi, D.; Tjong, S. C.; Li, R. K. Y. J Polym Sci Part B Polym Phys 2007, 45, 2674.
26. Yang, Z. G.; Zhang, Z. S.; Tao, Y. J.; Mai, K. C. J Appl Polym Sci 2009, 112, 1.
27. Yang, Z. G.; Mai, K. C. Thermochim Acta 2010, 511, 152.
28. Yang, Z. G.; Mai, K. C. J Appl Polym Sci 2011, 119, 3566.
29. Zhang, R. H.; Shi, D. A.; Tsui, C. P.; Tang, C. Y.; Tjong, S. C.; Li, R. K. Y. Polym Eng Sci 2011, 51, 403.
30. Göschel, U.; Lutz, W.Davidson, N. C. Compos Sci Technol 2007, 67, 2606.
31. Illers, K. H. Makromol Chem 1978, 179, 497.
32. Ozawa, T. Polymer 1971, 12, 150.
33. Xu, W.; Ge, M.; He, P. J Polym Sci Part B Polym Phys 2002, 40, 408.
34. Xu, W.; Zhai, H.; Guo, H.; Whitely, N.; Pan, W. P. J Therm Anal Calorim 2004, 78, 101.
35. Oburoglu, N.; Ercan, N.; Durmus, A.; Kasgoz, A. J Macromol Sci Part B Phys 2011, DOI:10.1080/00222348.2011.610231.
36. Avrami, M. J Chem Phys 1939, 7, 1103.
37. Avrami, M. J Chem Phys 1940, 8, 212.
38. Avrami, M. J Chem Phys 1941, 9, 177.
39. Jeziorny, A. Polymer 1978, 19, 1142.
40. An, Y.; Dong, L.; Mo, Z.; Liu, T.; Feng, Z. J Macromol Sci Part B Phys 1998, 36, 1305.
41. Zhang, U.; Zheng, H.; Lou, X.; Ma, D. J Appl Polym Sci 1994, 51, 51.
42. Supaphol, P.; Dangseeyun, N.; Simoon, P. Polym Test 2004, 23, 175.
43. Dobreva, A.; Gutzow, I. J Non-Cryst Solids 1993, 62, 1.
44. Dobreva, A.; Gutzow, I. J Non-Cryst Solids 1993, 62, 13.
45. Kim, S. H.; Ahn, S. H.; Hirai, T. Polymer 2003, 44, 5625.
46. Alonso, M.; Velasco, J. I.; De Saja, J. A. Eur Polym J 1997, 33, 255.
47. Papageorgiou, G. Z.; Achilias, D. S.; Bikiaris, D. N.; Karayannidis, G. P. Thermochim Acta 2005, 427, 117.
48. Oburoglu, N.; Ercan, N; Durmus, A.; Kasgoz, A. J Appl Polym Sci 2012, 123, 77.
49. Kissinger, H. E. J Res Natl Bur Stand 1956, 57, 217.
50. Zhao, X.-Y.; Zhang, B.-Z. J Appl Polym Sci 2010, 115, 1688.
51. Wang, B.; Wang, W.; Wang, H.; Hu, G. J Mater Sci 2010, 17, 429.